Flexible Dynamic Pressure Sensor for Insole Based on Inverse Viscoelastic Model

Abdo-Rahmane Anas Laaraibi, Gurvan Jodin, Damien Hoareau, Nicolas Bideau, Florence Razan

Flexible dynamic pressure sensor for insole based on inverse viscoelastic model

Abdo-rahmane Anas LAARAIBI[1,2,3], Gurvan JODIN[2,3], Damien HOAREAU[2,3] , Nicolas BIDEAU[4] and Florence RAZAN[1,2]

***Abstract*— The quantification of the plantar arch load and its surface distribution is essential to improve locomotion in many sports as well as rehabilitation protocols for patients. This paper has a threefold objective. First, it focuses on the design, fabrication and characterization of dynamic force sensors, based on both a single and multilayer of Velostat piezoresistive polymer. A matrix of 9 x 3 flexible pressure sensors has been developed to analyze and recognize plantar movements. Second, two models linking the plantar pressure to the resistance of the piezoresistive material, with and without taking into account the viscoelastic nature of the piezoresistive material, are proposed. Lastly, an inversion of the models is employed in order to estimate plantar pressure as a function of the variation in material resistance. An evaluation of the plantar pressure for various movements is also proposed.**

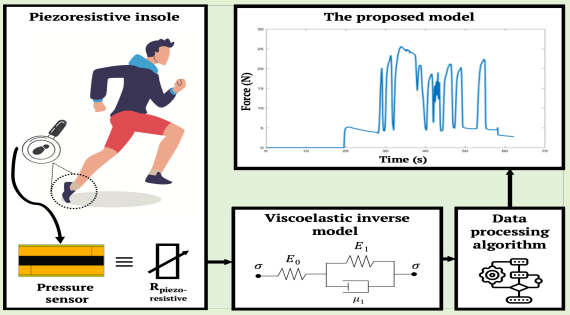

***Index Terms*— Piezoresistive sensors, Velostat, signal processing, viscoelasticity, dynamic modeling, sport sensor, plantar arch.**

I. Introduction

RECENTLY, foot plantar pressure measurement systems are attracting attention in biomedical and sports research fields, such as sports performance analysis [1], injury prevention [2] and rehabilitation [**?**].

Monitoring the distribution of foot plantar pressure during daily activities provides much useful biometric information related to both health condition and biomechanical performance. An analysis of this information serves to: develop customized footwear, improve sports performance, monitor a patient's rehabilitation status, and even detect early foot ulcers for diabetics [4]. To obtain information in an efficient and accurate manner, a variety of plantar pressure measurement systems have been designed.

The realm of commercial solutions encompasses capacitive sensors (Novel, Germany) [5], featuring Emed platform systems and Pedar systems installed in shoes, and resistive sensors (Tekscan, USA), e.g. MatScan platform systems and F-Scan footwear systems. On the other hand, piezoresistive sensors, e.g. FlexiForce (Tekscan, USA) [6], Vista Medical (Winnipeg, Manitoba, Canada) [7], and ParoTec (Paromed, Germany), are intended for professionals, researchers and physicians [8]. In addition, these sensors from Vista Medical, Novel and Tekscan have some performance limitations, such as price, repeatability, hysteresis and creep [9]. Also, some sensors (e.g. Parotec) display a limited pressure range and relatively large dimensions.

In addition to the actual commercial insole designs, studies have shown innovations in both structural layout and processing algorithms. The most common pressure detection mechanisms are listed in Table I.

Zhang et al. [10] developed a simple and low-cost insole for gait analysis, whose principle is mainly based on the capacitive mechanism using a force-sensing resistor (FSR) along with a commercial sensor. However, the FSR has poor accuracy and repeatability over the long term, while capacitive sensors exhibit nonlinear behavior, require additional electronic instrumentation and are sensitive to external noise. Charlon et al. [11] and Ivanov et al. [12] developed a smart insole capable of detecting the number of steps and performing the gait analysis using FlexiForce, which is in fact a commercial force sensor. Domingues et al. [13] presented a new optical fiber-based sensing architecture for the remote monitoring of foot plantar pressure distribution. This architecture contained Bragg gratings etched into the optical fiber so as to couple the optical response of a given wavelength to a localized fiber deformation, with the fiber acting as a strain gauges. De Fazio et al. [14] developed and produced a novel smart insole to monitor plantar pressure distribution using piezoresistive sensors.

These technical solutions have paved the way in the research of a plantar pressure detection system. However, they do display a number of performance limitations given that these insoles have not been modeled under both static and dynamic conditions, thus severely limiting practical applications.

This study is funded by the ANR within the framework of the PIA EUR DIGISPORT project (ANR-18-EURE-0022)

[1]OASIS, IETR UMR CNRS 6164, Avenue du Général Leclerc, Université de Rennes 1, Rennes 35042, France

[2]Department of Mechatronics, École normale supérieure de Rennes, Avenue Robert Schuman, Bruz 35170, France

[3]SATIE, UMR CNRS 8029, École normale supérieure de Rennes, 35170 Bruz, France

[4]M2S, École normale supérieure de Rennes, 35170 Bruz, France

E-mail:abdo-rahmane-anas.laaraibi@ens-rennes.fr(A.L), gurvan.jodin@ens-rennes.fr(G.J),damien.hoareau@ens-rennes.fr(D.H), nicolas.bideau@univ-rennes2.fr(N.B), florence.razan@ens-rennes.fr(F.R)

TABLE I
A COMPARISON OF PLANTAR PRESSURE DETECTION TECHNIQUES.

Mechanism	Strengths	Limitations
Piezoresistive	Low cost, simple structure and fabrication process, flexible, inexpensive and reliable for monitoring pressure distribution	Nonlinearity, repeatability, electronic instrumentation required
Piezoelectric	Flexible in size, large measuring range, high loading capacity	Not available for static measurements, false readings with vibrations, lower detection performance, repeatability, electronics required
Capacitive	Small size, high resolution, large sensing range, good repeatability	Alternative power supply, difficult implementation, expensive, sensitive to parasites
Optical Fibers	Low cost, good electrical insulation and electromagnetic field immunity, flexible, robust	Accuracy, requires measurement electronics and a data acquisition system
Inductive	High spatial resolution, multi-axis measurement of plantar pressure	Performance, robustness

This state-of-the-art allows for the following dual observation: 1) some commercial solutions are limited due to price and/or performance considerations, while a number of research efforts have yielded high detection performance but poor integration capabilities; and 2) piezoresistive sensors are low-cost, easy to integrate but not highly accurate. Models of accurate piezoresistive materials have been derived, yet they are currently inadequate, given that current data processing algorithms for piezoresistive insoles are basic with a low dynamic accuracy.

The aims of this study are to design, manufacture and modelize a low-cost, compact, smart and simply designed piezoresistive insole based on an inverse viscoelastic model.

For this purpose, the piezoresistive polymers, such as Velostat, have been modeled as a viscoelastic material using a spring and damper model, with the rationale behind this dynamic modeling step being to estimate the plantar force from resistance measurements using a data processing algorithm to improve sensor accuracy. Moreover, to verify the validity of the proposed model, various tests have been conducted on arbitrary and sports data. Ultimately, it has been demonstrated that the proposed model is accurate for estimating plantar pressure, as the higher precision will improve performance and prevent injuries to athletes.

The main contributions of this work are as follows:

- Design and characterization of a piezoresistive sensor and experimental set-up;
- Viscoelastic modelization of the piezoresistive sensors;
- Model inversion to estimate forces;
- Experimental calibration and characterization on non-sport specific data;
- Results on sports activity data (walking, running, change of direction).

The first part of this article presents the design and characterization of piezoresistive sensors within different structures. The main objective of the next part is to propose two models, with and without taking the viscoelastic effect into account; then, the viscoelastic model is reversed to estimate force as a function of measured resistance. The last part discusses the results obtained.

II. Materials and Methods

A. Working principle

The proposed sensor is based on an electroactive material, namely Velostat® (manufactured by 3M's Electronics Division, Saint Paul, USA) [16]. IIt features a piezoresistive material made of a polymer sheet (polyolefins) impregnated with carbon black to protect its components from electrostatic discharges (Table II). This device can be used in flexible electronics, portable electronics and matrix sensors in order to measure the force/weight distribution on the surface.

TABLE II
SELECTED MECHANICAL AND ELECTRICAL PROPERTIES.

Technical specifications	
Thickness	4 mil / 0.1mm thick
Temperature Limits	-45°C to 65°C (-50°F to 150°F)
Volume fraction of carbon particles	0.2873
Diameter of carbon particles (nm)	500
Volume Resistivity(ohm-cm)	$\leq$ 500

The piezoresistive effect refers to a change in the electrical resistivity of a semiconductor material or metal when a mechanical stress is applied, as shown in Fig. 1. In other words, the application of a force causes a decrease in the distance between the charge particles inside the Velostat, along with an increase in the number of conductive paths, which leads to a decrease in the resistance of the polymer.

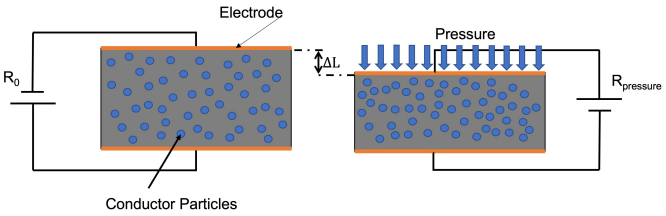

Fig. 1. Particles inside the materials are represented by blue circles; the effect of the applied pressure tends to change particle distances, with: $\boldsymbol{R_{pressure} < R_0}$.

The sensitivity of Velostat to applied pressure is primarily defined by two physical phenomena: quantum tunneling, and percolation [17]. Quantum tunneling affects the conductivity of a composite material when the distance between the conductive particles inside varies due to the applied pressure. The conductive particles can be electrically connected before the geometric connection. In contrast, percolation is a function of geometric characteristics. Percolation is correlated with a change in conductivity between the insulating and conducting states of a material, caused by a change in applied pressure [17].

A characterization of R vs. F of the piezoresistive material has been reported in [14], [15] and [18], as depicted in Fig. 2.

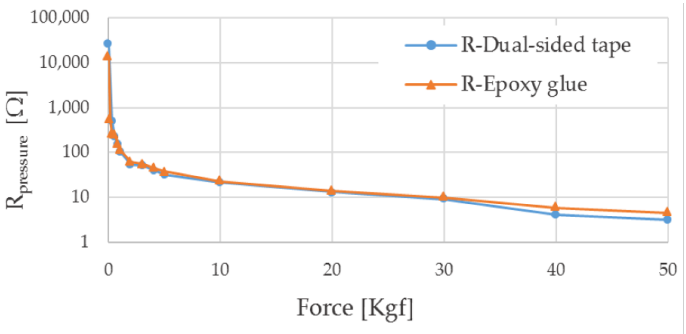

Fig. 2. Characteristics R vs. F (expressed in Kgf) for Velostat-based pressure sensor, extracted from [14].

A static sensor model without taking the viscoelastic effect into account is proposed in Equation 1.

$$R_{static} = (R_m - R_0) \cdot (\frac{0 - F_0}{F - F_0})^{\gamma} + R_0 \quad (1)$$

where, R_m is the maximum sensor resistance, R_0 the minimum sensor resistance, F_0 the sensor stiffness and γ the relaxation parameter, with F_0 and γ being constant parameters requiring identification.

Sensors can be single-point or matrices. For both types, three ways are available to generate a sensor structure according to [19], i.e.: (a) sandwich structure, (b) interdigital structure, and (c) fringe electrode structure. For our study, sensors were installed in a sandwich structure, as presented in Fig. 3, of size 4x4 cm^2 and a fulcrum of 1x1 cm^2 according to the test bench described below.

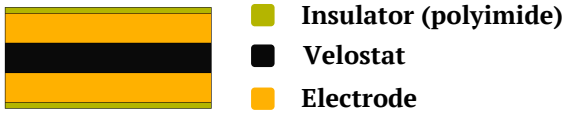

Fig. 3. The sandwich structure used to characterize the piezoresistive sensor.

B. Design and characterization of piezoresistive sensors and experimental setup

1) Force distribution on a insole: Since these sensors are designed to measure forces under the feet, it is appropriate to examine the distribution of forces. From the reference in [20], less pressure is shown to exist inside the arch of the foot and more pressure in the heel and forefoot, which remains less than 300 kPa. It can be deduced then that plantar pressure is mainly distributed in the heel, forefoot and toes; moreover, the force in the toe area is mainly concentrated on the big toe. Therefore, placing sensors at these locations can provide more relevant plantar pressure data, as listed below and seen in Fig. 4.

- The big toe (1) ;
- Metatarsal (2 & 3);
- Midfoot (4);
- Heel (5 & 6).

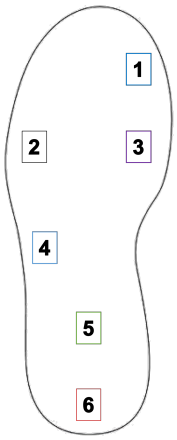

Fig. 4. Locations of interest for sensors on an insole. The black outline represents a left foot insole.

2) Sensor design: To characterize a piezoresistive pressure sensor, we first designed a sensor in a sandwich structure with a single active layer. This sensor is composed of 5 layers, as shown in Fig. 3. The electrodes supply voltage to the electroactive material (Velostat) and detect variations in resistance. The insulation cover protects against environmental interference and consolidates the sensor assembly.

The model is made up of an initial layer of Velostat in the middle with a thickness of 0.1 mm; then, two copper tapes 0.065 mm thick are placed above and below the Velostat without any adhesive between them and the electrodes. Lastly, two layers of adhesive insulators (polyimide) 0.076 mm thick are glued above and below the electrodes. In addition, this model proposes multilayer piezoresistive sensors, a new structure and a principle that calls for placing several layers of Velostat in series using an anisotropic conductive film (ACF) adhesive [21] between each layer to bond them. The underlying objective consists of increasing the resistance value of the piezoresistive sensor for better adequacy in conjunction with the conditioning electronics. Subsequently, we designed two types of multilayer sensors, as follows (Fig. 5):

- A multilayer sensor without the ACF adhesive (Fig. 5a),
- A multilayer sensor with an ACF adhesive (Fig. 5.b).

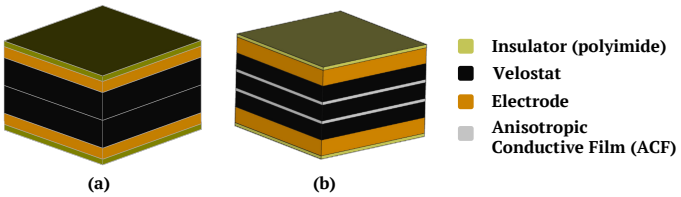

Fig. 5. The multilayer sandwich structure: (a) with 2 piezoresistive layers and without the anisotropic conductive film adhesive; and (b) with the anisotropic conductive film adhesive between the 3 piezoresistive layers.

ACF is an electrically anisotropic, conductive pressure-sensitive adhesive tape. This double-sided tape is loaded with silver particles that allow for interconnection through the adhesive thickness (z-axis) between the substrates. Contact is established between the adhesive and the Velostat by means of finger pressure at 15 psi (0.10 MPa).

For this case, the objective calls for using ACF to maintain electrical contact at all times, even without pressure, and achieving a higher resistance, which is advantageous for the electronic integration presented in the Results section below.

Next, we designed an insole equipped with a 9 x 3 matrix of sensors for foot pressure distribution measurements. This insole structure entails designing a five-layer sensor matrix with a single thickness of electroactive material, as explained in Fig. 6. It then becomes sufficient to measure the resistance between a row and a column in order to measure the resistance mainly located at the intersection and therefore choose the area of the insole to be addressed.

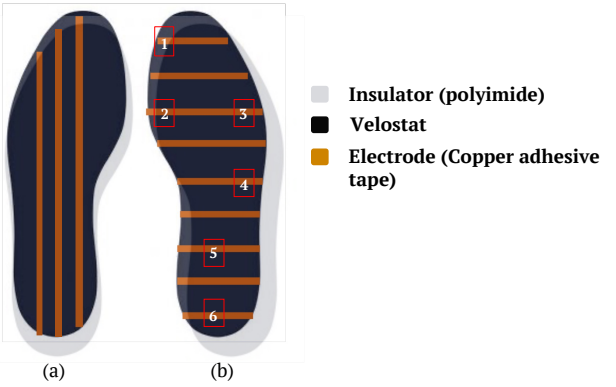

Fig. 6. A Velostat-based insole in matrix structure: (a) bottom view, (b) top view.

3) Test bench: These various prototypes have been characterized by a device allowing for the synchronous measurement of both the sensor resistance and the applied pressure force. We thus built a characterization test bench with a support target of 1x1 cm^2 ; moreover, the assembly is guided by a joint with a sufficiently large lever arm to assume that the target is being guided in vertical translation with little friction, as depicted in Fig. 7:

1) Receptacle for weights;
2) Load cell (500N);
3) Piezoresistive sensor (the sensor to be tested);
4) Acquisition card (Arduino Uno).

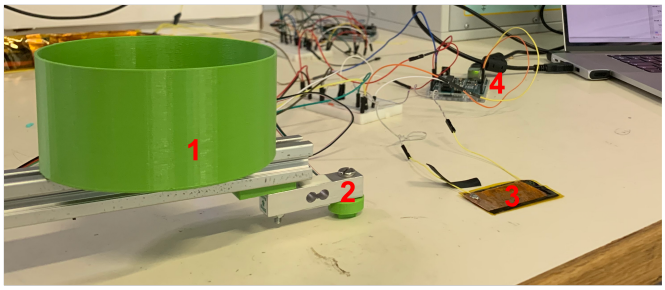

Fig. 7. The custom test bench for measuring the force and resistance of the piezoresistive sensor, 1: Receptacle, 2: Force sensor, 3: Piezoresistive sensor, and 4: Arduino uno.

This experimental device, diagrammed in Fig. 8, represents a lever arm that allows guiding the direction of the applied force, along with a receptacle for the weights and a 500-N force sensor to measure the applied force denoted F_{dir}, a piezoresistive sensor, and an acquisition board, Arduino Uno, for data acquisition. (The resistance measured by the Arduino Uno unit is denoted R_{dir}).

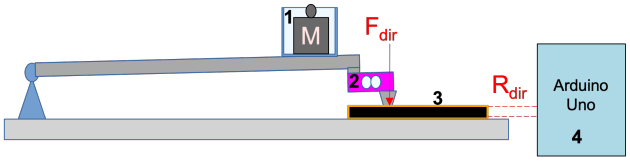

Fig. 8. Diagram of the test bench built (the number references correspond to those in Fig. 7.

To measure the sensor resistance, we implemented a voltage divider, in placing the sensor resistance, R_{dir}, in series with a fixed known reference resistor, R_1 as shown in Fig. 9. The analog input voltage of the A/D converter (Vs) can be derived by use of Equation 2:

$$V_s = V_{cc} \cdot \frac{R_{dir}}{R_{dir} + R_1} \tag{2}$$

where, V_s denotes the voltage at the sensor, V_{cc} the supply voltage, R_{dir} the sensor resistance, and R_1 the reference resistor.

A 470 Ohm is chosen for the reference resistor R_1 so as to maximize the amplitude of the output voltage over the entire range of variation of R_{dir} between 10 kOhm to 19 Ohm.

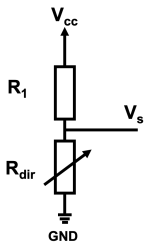

Fig. 9. The voltage divider circuit.

C. Viscoelastic modeling of piezoresistive sensors

After building the test bench, we were able to measure the sensor resistance R_{dir} (Ohms) and the applied force F_{dir} (N). The piezoresistive sensor was modeled to link the input force to the output resistor. The final goal here is to reverse this model to achieve a force estimator using the measured resistance R_{dir}.

We modeled the piezoresistive sensor as a standard linear solid viscoelastic model (shown in Fig. 10).

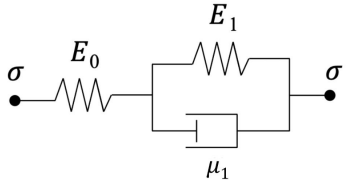

Fig. 10. Three parameter model of solids, or standard linear solid model.

This continuum mechanics model is based on a spring $E_0(Pa)$ in series with a parallel block, consisting of a spring $E_1(Pa)$

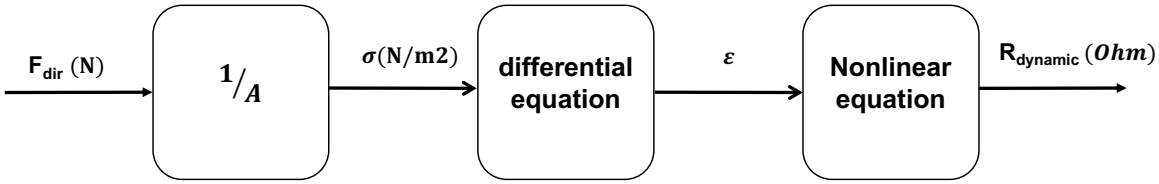

Fig. 11. The direct model of resistance $\boldsymbol{R_{dynamic}}$ as a function of force $\boldsymbol{F_{dir}}$, where $\boldsymbol{R_{dynamic}}$ denotes the resistance estimated by this model, $\boldsymbol{\varepsilon}$ the strain, $\boldsymbol{\sigma}$ the mechanical stress, and $\boldsymbol{F_{dir}}$ the force measured by a test bench.

and a damper $\mu_1(Pa/s)$, with $\sigma(N/m^2)$ the stress applied to this sensor. These coefficients are linear functions of the force.

A nonlinear behavioral equation links the piezoresistive sheet resistance to the strain. This relationship is assumed to be time-invariant; all dynamics are captured by the viscoelastic model, as described by Equation 3.

$$R_{dynamic} = R_0 \cdot (1 - \varepsilon) \cdot e^{-\theta \cdot \varepsilon} \tag{3}$$

where, $R_{dynamic}$ denotes the resistance estimated by viscoelastic model, R_0 the initial resistance of the sensor, ε the strain, and θ the relaxation parameter.

These viscoelastic models detailed in Algorithms 1 and 2 depend on the resistance of the piezoresistive sensor R_{dir}, the applied force F_{dir}, the stress σ, the strain ε, the elastic modulus of the springs E_0, the elastic modulus of the springs E_1 and the viscosity of the damper element μ_1 and the parameters of the non-linear equation 3.

For the parameter optimization of two models listed below, we used data sizes between 120 and 700 samples.

1) Direct model: The purpose of this first model is to estimate the resistance $R_{dynamic}$ as a function of F_{dir}, as measured by the test bench shown in Fig. 11. This model depends on the parameters of the model from Fig. 10, as well as on the stress σ and the strain ε found in Equations 4, 5 and 6.

$$\sigma = (E_1 \cdot \varepsilon_1) + (\mu_1 \cdot \dot{\varepsilon_1}) \tag{4}$$

$$\varepsilon = \varepsilon_0 + \varepsilon_1 \tag{5}$$

$$\varepsilon_0 = \frac{\sigma}{E_0} \tag{6}$$

From the Algorithm 1, we determined the stress as a function of F_{dir} and the area of the sensor denoted A; next, we used the implicit Euler method to solve the strain differential equation.

To estimate $R_{dynamic}$ of the model in Fig. 11, we need the values of the parameters E_0, E_1, μ_1 and θ. For this purpose, we posed the optimization problem as presented in Equation 7. To solve this problem, we relied on MathWorks MATLAB with the optimization toolbox 'fmincon' function. The "interior-point algorithm" was selected.

We optimized the four parameters (E_0, E_1, μ_1 and θ) by minimizing the mean square error (MSE) using the equation 7 between resistance R_{dir} (measured on the test bench) and resistance $R_{dynamic}$ calculated by our algorithm 1.

$$\underset{x}{\text{minimize}} \quad f_0(x) = \sum_{i=0}^{T} ||R^i_{dir} - R^i_{dynamic}(x)||^2 \tag{7}$$

Algorithm 1 direct model $R_{dynamic}$

1: **for** $i = 1, 2, \ldots, size(t)$ **do**
2: $\sigma(i) = F_{dir}(i)/A$
3: $E_0(i) = (E_{0a} \cdot F_{dir}(i)) + E_{0b}$ ▷ Elastic modulus of the spring E_0
4: $E_1(i) = (E_{1a} \cdot F_{dir}(i)) + E_{1b}$ ▷ Elastic modulus of the spring E_1
5: $\mu_1(i) = (\mu_{1a} \cdot F_{dir}(i)) + \mu_{1b}$ ▷ Viscosity of the damper μ_1
6: $\varepsilon_1(i+1) = \varepsilon_1(i) + \frac{dt}{\mu_1(i)} \cdot (\sigma(i) - (E_1(i) \cdot \varepsilon_1(i)))$ ▷ Implicit Euler method of equation 4
7: $\varepsilon(i) = \frac{\sigma(i)}{E_0(i)} + \varepsilon_1(i)$ ▷ equation 5 & equation 6
8: $R_{dynamic}(i) = R_0 \cdot (1 - \varepsilon(i)) \cdot e^{-\theta \cdot \varepsilon(i)}$
9: **end for**

with: t: time vector, A: area, dt: time step,

2) Inverse model: To use the sensor, it is necessary to invert the direct model to estimate the value of the force that produced the measured resistance value. For this purpose, using the inverse model shown in Fig. 12, we estimated the force $F_{dynamic}$ as a function of the resistance R_{dir}, optimized parameters (E_0, E_1 and μ_1), the strain ε and the stress σ.

Using the same optimized parameters (E_0, E_1, μ_1 and θ) in the direct model and from the Algorithm 2, we started by finding the strain ε in function of R_{dir}, R_0 and θ applying Equation 8 by means of the trust region dogleg method available on MathWorks MATLAB 2021a software.

$$R_0 \cdot (1 - \varepsilon) \cdot e^{-\theta \cdot \varepsilon} - R_{dir} = 0 \tag{8}$$

Afterwards, we used the implicit Euler method to solve the standard linear solid model by Equations 9 and 10 to find the stress σ.

$$\sigma = (\varepsilon - \varepsilon_1) \cdot E_0 \tag{9}$$

$$\sigma = (E_1 \cdot \varepsilon_1) + (\mu_1 \cdot \dot{\varepsilon_1}) \tag{10}$$

Similarly, the cost function consists in minimizing the MSE between F_{dir} (measured on the test bench) and $F_{dynamic}$ calculated by Algorithm 2 (see Equation 11).

$$\underset{x}{\text{minimize}} \quad f_0(x) = \sum_{i=0}^{T} ||F^i_{dir} - F^i_{dynamic}(x)||^2 \tag{11}$$

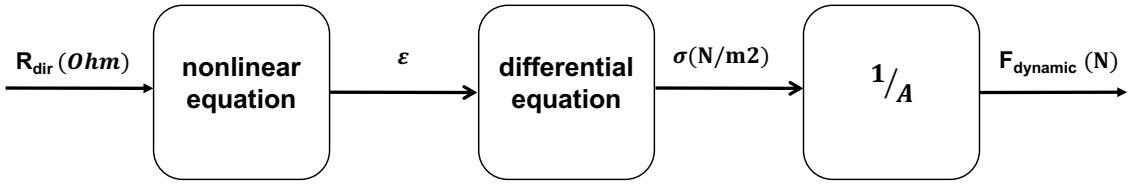

Fig. 12. The inverse model of force $\boldsymbol{F_{dynamic}}$ as a function of $\boldsymbol{R_{dir}}$, where $\boldsymbol{F_{dynamic}}$ represents the force estimated by this model, $\boldsymbol{\varepsilon}$ the strain, $\boldsymbol{\sigma}$ the mechanical stress, and $\boldsymbol{R_{dir}}$ the resistance measured by a test bench.

Algorithm 2 inverse model $F_{dynamic}$

find ε in function of R_{dir}, R_0 et θ
for $i = 1, 2, \ldots, size(t)$ **do**
  $\sigma(i+1) = \sigma(i)$
  $E_0(i) = (E_{0a} \cdot \sigma(\mathrm{i}) \cdot A) + E_{0b}$
    ▷ Elastic modulus of the spring E_0
  $\mathrm{E}_1(i) = (E_{1a} \cdot \sigma(\mathrm{i}) \cdot A) + E_{1b}$
    ▷ Elastic modulus of the spring E_1
  $\mu_1(i) = (\mu_{1a} \cdot \sigma(i) \cdot A) + \mu_{1b}$
    ▷ Viscosity of the damper μ_1
  ε = argmin (equation 10)
    ▷ Implicit Euler method
  $\sigma(i+1) = (\varepsilon - \varepsilon_1) \cdot E_0$
    ▷ equation (9)
  $F_{dynamic}(i+1) = \sigma(i+1) \cdot A$
end for
With: t: time vector, A: area, dt: the time step.

The goal of this algorithm is to estimate the force from the resistance measurement of the piezoresistive sensor, with the force sensor being used as a reference sensor, hence the plantar pressure in an insole can be easily measured.

An initial dataset was used for optimization of the E_0, E_1, μ_1 and θ parameters and then other datasets were used to evaluate the sensor performance, according to the method described above. Moreover, we calculated the normalized error (see Equation 12). The force was normalized by 30 N because this is the typical maximum amplitude of a force under the foot, as noted in Section II-B, along with the mean square error (MSE), as stated in Equations 7 and 11.

$$err(\%) = \frac{F_{dynamic} - F_{dir}}{30} \cdot 100 \qquad (12)$$

Regarding the datasets and optimization procedure, the parameters were initially optimized with an arbitrary force dataset using the direct model. The resulting optimized parameters were then validated for the inverse model, and no newly optimized parameters were needed for the non-sports data. Yet this set-up can be refined in order to improve sensor accuracy; this is accomplished by optimization in keeping the original value of θ. The reason for reoptimizing these parameters is that sports data feature various dynamics and amplitudes.

D. Sport dataset

Using a commercial Moticon® insole, we repeated the same types of movements (walking, running, changing direction) with the test bench, in taking into account the amplitude and frequency for each type of data.

Similarly, and as explained in Section II-C.2, we assigned a value of θ and optimized the parameters of the standard linear solid model using directional change type of data on a 168-sample size and then testing the run and walk type of data on sample sizes of 204 and 344, respectively, as illustrated in Fig. 19.

III. Results

This section presents the experimental results on piezoresistive sensors tested under both static and dynamic conditions.

A. Characterization under static conditions

We started by characterizing the single-layer piezoresistive sensor under static conditions, as described in Equation 1. This result is presented in Fig. 13.

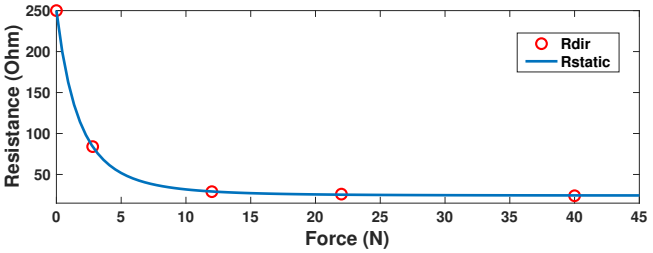

Fig. 13. Static characterization of the piezoresistive sensor in a single layer.

The characterization of the piezoresistive sensor consisted of applying a load for 4 min before measuring the resistance that serves to obtain a stable value; next, the load was removed from the sensor, in waiting 3-4 min before repeating this same step. Thus, 5 different measurement tests were performed for the sensors studied, with the dispersion and mean being calculated.

Similarly, the following multilayer piezoresistive sensors were characterized:

- 3-layer sensor with an anisotropic conductive adhesive film (ACF);
- 3-layer sensor without the ACF adhesive;
- 2-layer sensor with the ACF adhesive;
- 2 layer sensor without the ACF adhesive.

The results obtained are displayed in Fig. 14. The qualitative behavior is very similar, as evidenced by perfectly detecting the resistance variations as a function of the force being exerted on each of the sensors. From these and other equivalent tests,

not discussed herein for purposes of brevity, we are able to observe that the behavior of the sensors is very similar. In addition, the multilayer sensors with the ACF adhesive provide greater resistance compared to the multilayer sensors without this adhesive, which offers an advantage in designing the signal amplifier.

Thus, the multilayer sensors without ACF exhibit less linear behavior, with a high sensitivity of resistance for low forces. Moreover, we conclude that repeatability is the major unresolved problem of Velostat due to the differences observed on the 5 tests, as illustrated in Fig. 14.

In the literature, researchers stopped at this point, without taking into account the viscoelastic effect of the piezoresistive material.

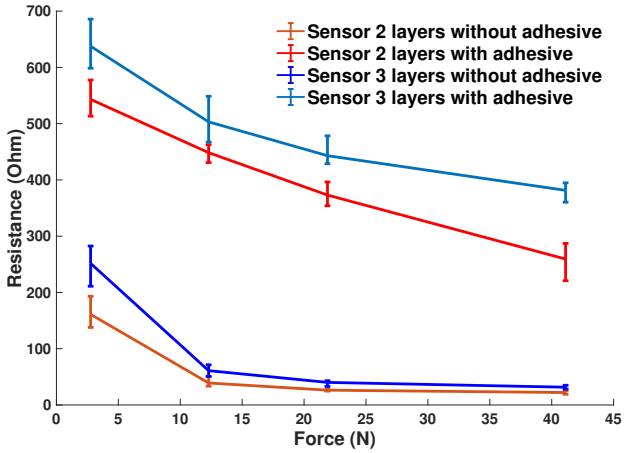

Fig. 14. Static characterization of multilayer sensors both with and without the ACF adhesive (error bars representing min and max).

B. Dynamic viscoelastic model

This section will present the results of the single-layer sensor for both the direct and inverse models. Two kinds of forces are applied: an arbitrary varying force, and sports data collected by a commercial insole.

1) Direct model: For this section, the direct algorithm described in Section II-C.1 is applied. An initial dataset is used for parametric optimization; then, other datasets will be introduced to evaluate sensor performance. Fig. 15, with an arbitrary test dataset, shows: the force F_{dir} measured by the test bench, the resistance R_{dir} of the single-layer sensor, $R_{dynamic}$ the resistance estimated by the direct model algorithm, and R_{static} the resistance computed by the optimized static model in Equation 1.

The upper curve (Fig. 15a) shows the force applied to the sensor vs. time. The force initially equals zero, then a first low tray is applied before achieving dynamic variations. The following plots (Fig. 15b) show the measurement and resistance models at the same time. In particular, let's note that resistance decreases as force increases.

From these results, the immediate step response of the static model can be observed, while the dynamic model better follows the dynamic response of the R_{dir} measurement. Furthermore, we have find a root mean square error MSE = 8.75 Ohms for

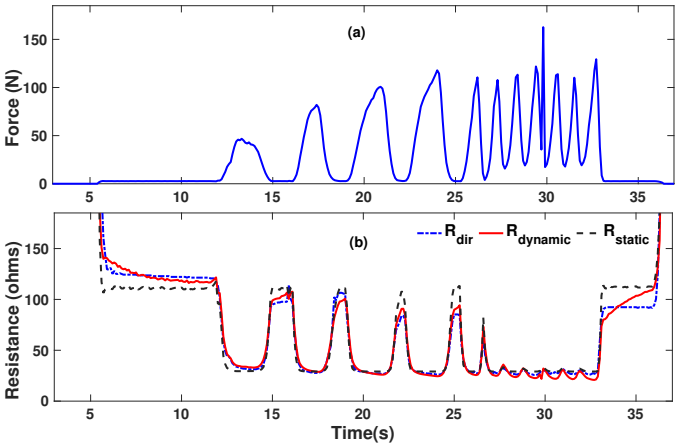

Fig. 15. (a): The force $\boldsymbol{F_{dir}}$ measured on the test bench (Non-sport specific data), (b): The experimental resistance $\boldsymbol{R_{dir}}$, $\boldsymbol{R_{static}}$ and the resistance of the direct dynamic model $\boldsymbol{R_{dynamic}}$ versus time.

the dynamic direct model and an MSE = 12.8765 Ohms for the static model.

The histogram of the error is presented in Fig. 16; it clearly indicates that the proposed dynamic model is more accurate than the state of the art.

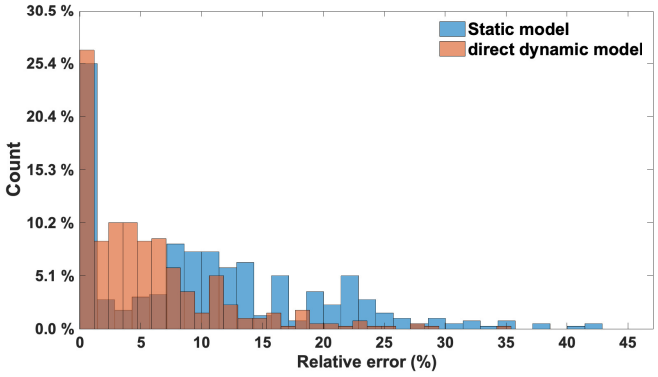

Fig. 16. Histogram of the error of both the static model and the dynamic direct model of the same dataset used in Fig. 15.

From the dataset in Fig.15, we derived the standard linear solid model parameters for the direct single-layer sensor model as follows for θ = 3.49:

$$E_0(Pa) = (2.2429 \cdot 10^4) \cdot F_{dir}(N) + 8.3658 \cdot 10^4 \quad (13)$$

$$E_1(Pa) = (5.7960 \cdot 10^4) \cdot Fdir(N) + 3.8400 \cdot 10^5 \quad (14)$$

$$\mu_1(Pa/s) = (3.2864 \cdot 10^5) \cdot Fdir(N) + 3.8442 \cdot 10^4 \quad (15)$$

2) Inverse model: This part estimates the applied force $F_{dynamic}$ as a function of the resistance of the piezoresistive sensor R_{dir}, with the objective being to integrate this force estimator in the insole presented earlier. First, let's follow the same steps from Section II-C.2 using the inverse algorithm and on two types of data:

- **Non-sports specific tests**:

The inverse algorithm is applied here on non-sports specific data. With this same method, we use the parameters optimized

by the direct model on the dataset presented in Fig. 17 and apply them on other test data.

From the results of Fig. 17 and Fig. 18, we can see that our inverse algorithm accurately estimates the applied force with a mean square error (MSE) equal to 2.66 N. This error is calculated solely with the validation data, which exclude the optimization datasets. This good result gets tested for arbitrary manual force inputs. The next section will focus on sports force inputs.

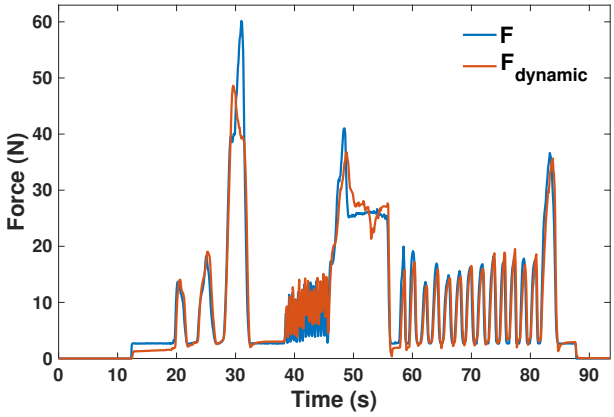

Fig. 17. The experimental force $\boldsymbol{F_{dir}}$ and dynamic force of the inverse model $\boldsymbol{F_{dynamic}}$ vs. time.

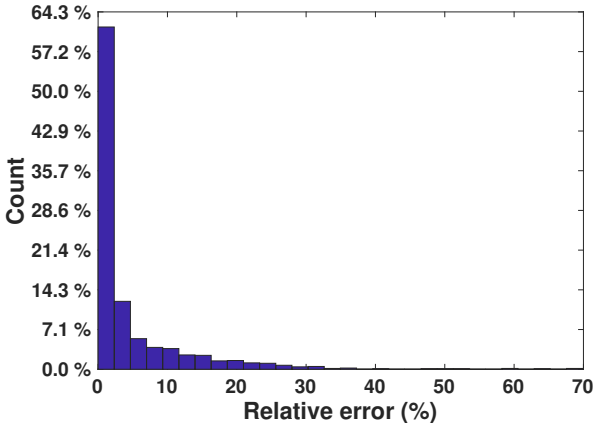

Fig. 18. Histogram of non-sports specific data error (Fig.17).

- **Sports specific tests (walking, running and changing direction)**:

The amplitudes and dynamics of these signals differ from actual insole signals. For this reason, we have opted to test them on data dedicated to sports, as presented in the following section.

$$E_0(Pa) = [(6.59 \cdot 10^4) \cdot \sigma(N/m^2) \cdot A(m^2)] + 10^6 \quad (16)$$

$$E_1(Pa) = [(3 \cdot 10^4) \cdot \sigma(N/m^2) \cdot A(m^2)] + 6.23 \cdot 10^6 \quad (17)$$

$$\mu_1(Pa/s) = [(1 \cdot 10^4) \cdot \sigma(N/m^2) \cdot A(m^2)] + 3.69 \cdot 10^5 \quad (18)$$

From the results obtained, as illustrated in Fig. 19, it is apparent that our inverse algorithm is able to estimate plantar pressure (force applied by the foot) with a mean square error (MSE) calculated from validation data by type of application of: 6.95 N for a change in direction, 5.73 N for running, and 4.74 N for walking.

In addition, from our calculation of the relative error, as shown in Fig. 20, we can observe that much of the error is less than 2%, which is due for example to the fact that the force often equals zero for the walking application.

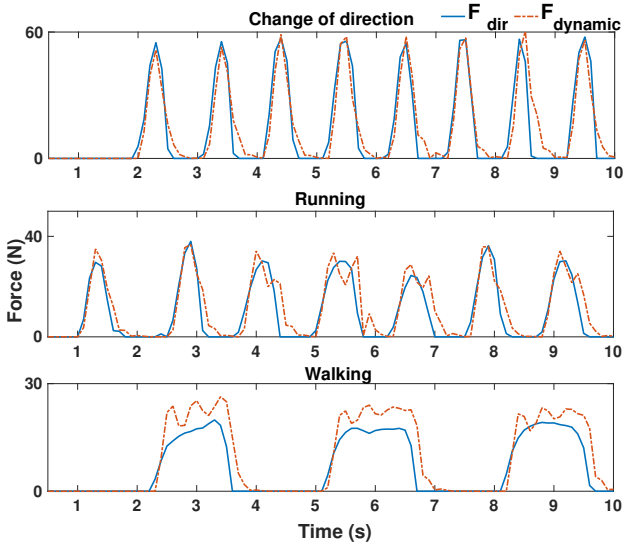

Fig. 19. The experimental force $\boldsymbol{F_{dir}}$ and the dynamic force of the inverse model $\boldsymbol{F_{dynamic}}$ vs. time (sports type data: change of direction, running, walking).

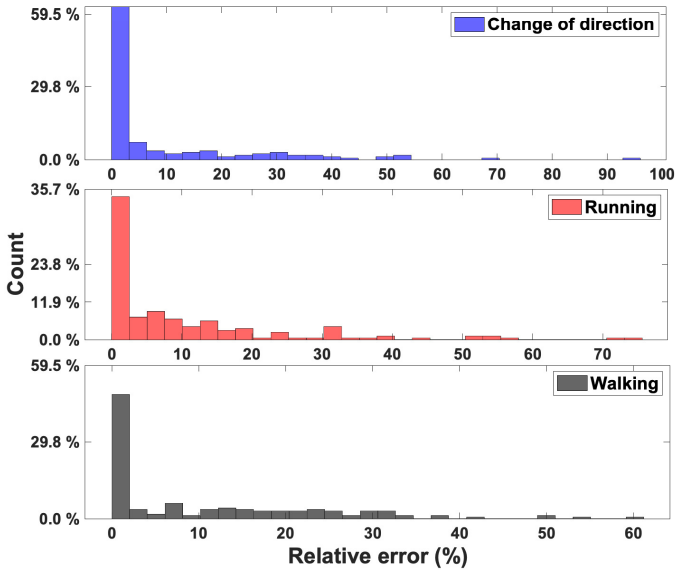

Fig. 20. Histogram of the sports type data error: changing direction, running, walking.

The Bland Altman diagram (Fig. 21) plots the deviations between the reference sensor and the piezoresistive sensor measurements once the inverse viscoelastic model has been applied. These deviations are plotted as a function of the measurement amplitude (i.e. average between the reference and piezoresistive sensors). These amplitudes and deviations are plotted on a logarithmic scale so as to avoid that the larger values

take precedence over the smaller ones. This graph exacerbates the deviations and exposes the performance of the piezoresistive sensor as a function of the applied force amplitude; it is seen here that the tested forces are quite homogeneous within the force range, despite a slightly higher concentration around a value corresponding to 4 N (at the weight of the load cell when placed on the piezoresistive sensor). Also, this graph shows that the estimated force has been underestimated for the larger values.

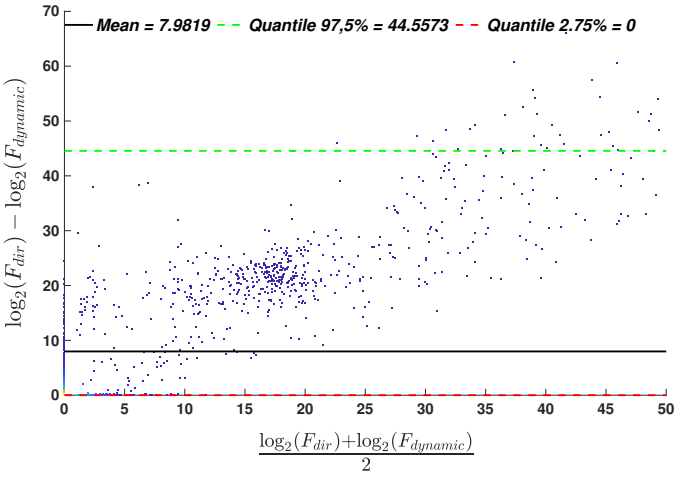

Fig. 21. Bland Altman diagram of sports type data: change of direction, running, walking.

IV. Conclusion & perspectives

Several Velostat-based piezoresistive sensors for various structures have been produced and tested in this study. According to test results, it can be concluded that multilayer sensors with ACF adhesive display better sensitivity compared to the multilayer format without ACF. A viscoelastic model has been developed and then inverted to obtain the plantar pressure from resistance measurement of the piezoresistive material. The model parameters have been optimized for sports data, such as walking, running and changing direction. Lastly, the development of this model has improved the accuracy of the piezoresistive sensors, in paving the way to achieve inexpensive and accurate dynamic plantar pressure measurements in the sports field, which entails high intensity, and dynamic and multidirectional loads. To achieve this aim, the next step would be to encapsulate the insole. Subsequently, the effect of temperature, voltage and excessive vibration on these sensors would need to be examined.

References

[1] T. Holleczek, A. Ru, H. Harms, and G. Tro, "Textile pressure sensors for sports applications," in 2010 IEEE Sensors, Kona, HI: IEEE, Nov. 2010, pp. 732–737, isbn: 978-1-4244-8170-5. doi: 10.1109/ICSENS.2010.5690041. (visited on 20/04/2022).

[2] S. Mansfield, K. Obraczka, and S. Roy, "Pressure injury pre- vention: A survey," IEEE Reviews in Biomedical Engineering, vol. 13, pp. 352–368, 2020, issn: 1937-3333, 1941-1189. doi: 10.1109/RBME.2019.2927200. (visited on 20/04/2022).

[3] E. Simonetti, E. Bergamini, C. Villa, J. Bascou, G. Vannozzi, H. Pillet. "Gait events detection using inertial measurement units in people with transfemoral amputation: a comparative study,"Medical & Biological Engineering & Computing, 58:461–470 (2020). doi: 10.1007/s11517-019-02098-4 (visited on 20/04/2022)

[4] C. A. Abbott, K. E. Chatwin, P. Foden, et al., "Innovative intelligent insole system reduces diabetic foot ulcer recurrence at plantar sites: A prospective, randomised, proof-of-concept study," The Lancet Digital Health, vol. 1, no. 6, e308–e318, Oct. 2019, issn: 25897500. doi: 10.1016/S2589-7500 (visited on 05/05/2022).

[5] Novel. (), [Online]. Available: http : / / www . novel . de/. (visited on 20/04/2022).

[6] Tekscan. "Tactile pressure measurement,pressure mapping sys- tems,force sensors and measurement systems." (), [Online]. Available: http : / / www . tekscan . com/. (visited on 20/04/2022).

[7] Vista. "Medical home of pressure mapping, pressure imaging and pressure sensing." (), [Online]. Available: http://www. pressuremapping.com/. (visited on 20/04/2022).

[8] Paromed. (), [Online]. Available: http://www.paromed.de/. (visited on 20/04/2022).

[9] A. H. Abdul Razak, A. Zayegh, R. K. Begg, and Y. Wahab, "Foot plantar pressure measurement system: A review," Sensors, vol. 12, no. 7, pp. 9884–9912, Jul. 23, 2012, issn: 1424-8220. doi: 10.3390/s120709884. (visited on 10/12/2021).

[10] Q. Zhang, Y. L. Wang, Y. Xia, X. Wu, T. V. Kirk, and X. D. Chen, "A low-cost and highly integrated sensing insole for plantar pressure measurement," Sensing and Bio-Sensing Research, vol. 26, p. 100 298, Nov. 2019, issn: 22141804. doi: 10.1016/j.sbsr.2019.100298 (visited on 20/04/2022).

[11] Y. Charlon, E. Campo, and D. Brulin, "Design and evaluation of a smart insole: Application for continuous monitoring of frail people at home," Expert Systems with Applications, vol. 95, pp. 57–71, Apr. 2018, issn: 09574174. doi: 10 . 1016 / j . eswa . 2017 . 11 . 024. (visited on 20/04/2022).

[12] K. Ivanov, Z. Mei, L. Lubich, et al., "Design of a Sensor Insole for Gait Analysis," H. Yu, J. Liu, L. Liu, Z. Ju, Y. Liu, and D. Zhou, Eds., pp. 433–444, 2019. (visited on 10/05/2022).

[13] M. F. Domingues et al., "Insole Optical Fiber Sensor Architecture for Remote Gait Analysis—An e-Health Solution," in IEEE Internet of Things Journal, vol. 6, no. 1, pp. 207-214, Feb. 2019, doi: 10.1109/JIOT.2017.2723263. visited on 28/11/2022).

[14] R. de Fazio, E. Perrone, R. Velázquez, M. De Vittorio, and P. Visconti, "Development of a self-powered piezo-resistive smart insole equipped with low-power BLE connectivity for remote gait monitoring," Sensors, vol. 21, no. 13, p. 4539, Jul. 1, 2021, issn: 1424-8220. doi: 10.3390/s21134539. (visited on 10/12/2021).

[15] M. Kalantari, J. Dargahi, J. Kövecses, M. G. Mardasi, and S. Nouri, "A new approach for modeling piezoresistive force sensors based on semiconductive polymer composites," IEEE/ASME Transactions on Mechatronics, vol. 17, no. 3, pp. 572–581, Jun. 2012, issn: 1083-4435, 1941-014X. doi: 10.1109/TMECH.2011.2108664. (visited on 12/10/2021).

[16] 3M. "Film, Velostat, 36 x 150 roll 67y8891." (), [On- line]. Available: https : / / datasheet . octopart . com / 170436X150- SCS- datasheet-15984175.pdf/. (visited on 20/04/2022).

[17] A. Dzedzickis, E. Sutinys, V. Bucinskas, et al., "Polyethylene- carbon composite (Velostat) based tactile sensor," Polymers, vol. 12, no. 12, p. 2905, Dec. 3, 2020, issn: 2073-4360. doi: 10 . 3390 / polym12122905. [Online]. Available: https : / / www . mdpi . com / 2073 - 4360 / 12 / 12 / 2905 (visited on 10/05/2022).

[18] D. A. Valle-Lopera, A. F. Castraño-Franco, et al., "Test and fabrication of piezoresistive sensors for contact pressure measurement," Revista Facultad de Ingeniería Universidad de Antioquia, no. 82, pp. 47–52, Mar. 2017, issn: 01206230. doi: 10 . 17533 / udea . redin . n82a06. (visited on 12/10/2021).

[19] D. Giovanelli and E. Farella, "Force sensing resistor and evaluation of technology for wearable body pressure sensing," Journal of Sensors, vol. 2016, pp. 1–13, 2016, issn: 1687- 725X, 1687-7268. doi: 10.1155/2016/9391850. (visited on 12/10/2021).

[20] E. Klimiec, B. Jasiewicz, J. Piekarski, K. Zaraska, P. Guzdek, and G. Ko laszczyński, "Measuring of foot plantar pres- sure—possible applications in quantitative analysis of hu- man body mobility," Measurement Science and Technology, vol. 28, no. 5, p. 054 008, Apr. 2017, issn: 0957-0233, 1361- 6501. doi: 10.1088/1361- 6501/aa60a9. (visited on 19/05/2022).

[21] ACF. (), [Online]. Available: https://fr.rs-online.com/web/p/adhesifs/2209928. (visited on 25/04/2022).

Abdo-rahmane Anas LAARAIBI was born in Casablanca, Morocco in 1996. He received his first M.S degree in Automation-Signal Processing-Computer Science from Hassan 1er University, Settat, MA in 2020 and his second M.S degree in Signal Image from Rennes 1 University, Rennes, FR in 2021. He is currently a PhD student in Mechatronic Engineering at Ecole Normale Supérieure de Rennes, IETR group and SATIE laboratory of Rennes.

His research focuses on the development of an autonomous integrated instrumentation allowing the quantification of an athlete's movements for indoor sports

Gurvan JODIN received the B.S. in both mechanical engineering and electrical engineering, from Rennes 1 University, France, in 2011. He received the M.Ed in mechatronics from Ecole Normale Supérieure de Rennes, and was major of the 2013 "agrégation" teacher competitive recruitment of Industrial Science for Engineering. He received the Ph.D. degree from Polytechnic National Institute of Toulouse, France, in electrical engineering and aerodynamics. After postdocs at Mechanical Engineering Department at Massachusetts Institute of Technology, Boston, MA, USA, and at Ecole Normale Supérieure de Rennes, he is currently associate professor with SATIE laboratory at Ecole Normale Supérieure de Rennes, France. His research interests are in eco-co-design complex mechantronics systems. This includes topics in experimental approach, mechatronics, hydrodynamics, sensors, power electronics and smart grids.

Damien HOAREAU received the B.S. degree in mechanical and electrical engineering from Rennes 1 University and Ecole Normale Supérieure de Rennes, Rennes, France, in 2017 and the M.S. degree in complex engineering system from Rennes 1 University and Ecole Normale Supérieure de Rennes, Rennes, France, in 2020. He is currently pursuing the Ph.D. degree in engineering science at Ecole Normale Supérieure de Rennes, Rennes, France.

His research interest includes the development of sensing system for sport science and signal processing to monitor athelete parameters to improve performance.

Nicolas BIDEAU was born in France in 1978. He received the bachelor degree in Mathematics from the University of Brest, France, the applied mathematics degree and the mechanics degree from the university Rennes 1. He received the PhD degree in Mechanics from the University Rennes 1, France, in 2009. In 2009 he joined the University of Technology of Compiègne, France as a postdoctoral researcher in biomedical engineering. Since 2011, he is an assistant professor in biomechanics at the department of sports sciences from the University Rennes 2. His current research interests, as member of the Movement, Sports and Health (M2S) laboratory, include movement analysis, modeling end experimental biomechanics with applications to sports sciences. His main applications focus on biomechanical analysis of the musculoskeletal system from optoelectronic or IMU based motion capture as well as the analysis of the athlete's material and environmental interactions.

Florence RAZAN received a master in physic and electronic in 2002 and a PhD in microsystems of Bordeaux University (France) in 2005. From 2006 to 2020, she was an associate professor with the mechatronic department at ENS Rennes and in SATIE laboratory. She is currently professor at ENS Rennes and IETR group. Her teams interest concerns the development of autonomous biosourced microsystems for movement characterization. Her current work focuses on the development of autonomous and biosourced embedded communicating systems as an interface between humans or humanoid robots and their environment. The main challenges concern the system architecture, the design of autonomous sensors, the integration of an energy recuperator and the development of low-power electronics. Her main research interests focuse on the development of piezoelectric transducers.